Investigation of Case II Diffusion Behavior. 1. Theoretical Studies Based on the Relaxation Dependent Solubility Model

M. Sanopoulou, D. F. Stamatialis,† and J. H. Petropoulos*

Physical Chemistry Institute, Demokritos National Research Center, GR-15310 Aghia Paraskevi, Athens, Greece

Received August 9, 2000; Revised Manuscript Received June 18, 2001

ABSTRACT: A model previously shown to provide physically meaningful interpretation of a wide range of polymer−penetrant relaxation-induced non-Fickian (including case II) sorption kinetics, is used here as a basis for a deeper understanding of fundamental case II kinetic features. In particular, we report and discuss model calculation results on the dependence of penetration velocity v, and of important characteristics of the concentration profile, on the main material parameters which characterize the system. The latter include the polymer relaxation rate constant relative to the diffusion constant, the parameters measuring the magnitude of the (exponential) concentration dependence of these constants, and the sorptive capacity of unrelaxed, relative to relaxed, polymer. A precisely defined relaxation lifetime is evaluated analytically and shown to provide a simple single-parameter link between penetration velocity behavior and relaxation kinetics. In the same vein, a quantitative measure of the steepness of the sharp penetration front, also amenable to analytical evaluation, is proposed and its application illustrated.

Introduction

The term "case II diffusion" was first applied by Alfrey et al.[1] to micromolecular penetration into a glassy polymer substrate characterized by zero-order kinetics and a sharp penetrant advancing front. This phenomenon appeared to constitute a limiting form of the deviation from normal Fickian penetration kinetics (correspondingly termed "case I diffusion") commonly exhibited by glassy polymer-micromolecular penetrant systems. It was first shown by Crank,[2] on the basis of suitable simplified models, that such non-Fickian (NF) sorption kinetics could plausibly be attributed to penetrant-induced slow viscous molecular relaxation (VR) and/or differential swelling stresses (DSS) in the swelling polymer substrate.

The intense interest in the study of case II diffusion stimulated by the work of Alfrey et al.[1] soon led to the realization that it constitutes an extreme form of relaxation- controlled penetration kinetics.[3] Even so, the demonstration that case II behavior could be predicted theoretically on the basis of the fundamental model formulations originally proposed by Crank[2] came after a rather long period of time[4−6] (during this period, NF diffusion theory could deal with this phenomenon only empirically by postulating the presence of a case II convection process occurring simultaneously with Fickian diffusion).[3,7,8] The particular modeling approaches[4−6] used for this purpose differ from those of Crank[2] in two significant respects; namely (i) the necessity (first emphasized in ref 9) to formulate the diffusion process in terms of a chemical potential gradient (instead of a concentration gradient) driving force was recognized and (ii) the sorptive capacity of the polymer for the penetrant (rather than the diffusivity of the latter in the polymer)[2] was considered as the property primarily affected by the underlying physical mechanism(s). Thus, the operative diffusion equation for unidimensional liquid penetration into a seminfinite dry polymer film is[4−8]

$$\frac{\partial C}{\partial t} = \frac{\partial}{\partial x}\left(D_T \frac{C}{a}\frac{\partial a}{\partial x}\right) \equiv \frac{\partial}{\partial x}\left(D_T S \frac{\partial a}{\partial x}\right) \qquad (1a,b)$$

with

$$a(x = 0, t) = 1, \quad a(x, t = 0) = 0, \quad a(x \to \infty, t) = 0 \qquad (2a,b,c)$$

In eqs 1 and 2, x denotes position along the axis of penetration with $x = 0$ at the surface exposed to bulk liquid, t is the time, D_T is the thermodynamic diffusion coefficients defined here on a polymer-fixed frame of reference, C is the concentration of penetrant in the polymer at given x and t (in mol per unit volume of pure polymer), and a is the corresponding activity defined by

$$\mu = \mu^o + RT \ln a \qquad (3)$$

where μ, μ^o represent the chemical potential of penetrant in the polymer and in the pure bulk liquid, respectively. In eq 1b, $S \equiv C/a$ is the solubility coefficient, defined as a measure of the sorptive capacity of the polymer at any given stage of the relaxation process; hence the designation "time-dependent solubility" (TDS) model adopted in ref 5, to distinguish this approach from the "time-dependent diffusivity" (TDD) one used by Crank[2] (but note that the terms "relaxation-dependent solubility or diffusivity" would provide a more accurate description of the nature of these models). In all cases, ideal sorption of the penetrant by the polymer was assumed for the sake of simplicity [this was done by setting $S(a) = S(a = 1)$; see below], while D_T was a strong increasing function of C.

The treatments of Thomas and Windle (TW)[4] and of Petropoulos (JP)[5] differ in their formulation of the viscous relaxation process. In the former approach, this process (a) is assumed to control penetrant uptake fully

* Corresponding author. Telephone: +30-1-6503785. Fax: +30-1-6511766. E-mail: petrop@mail.demokritos.gr.

† Present address: European Membrane Institute Twente, University of Twente, Chemical Technology Department, P.O. Box 217, NL-7500 AE Enschede, The Netherlands 1.

10.1021/ma001408j CCC: $22.00
Published on Web 01/22/2002

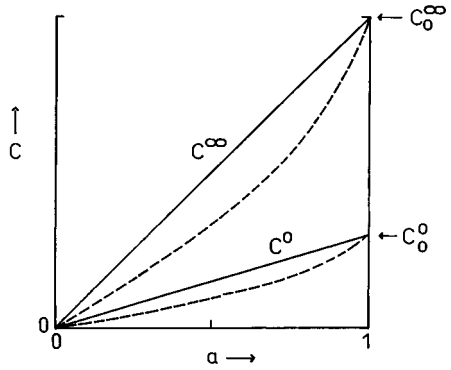

Figure 1. Schematic representation of actual (- - -) and linearized (−) sorption isotherms for unrelaxed [$C^o(a)$] and fully relaxed [$C^\infty(a)$] polymer.

(i.e., unrelaxed polymer cannot take up *any* penetrant) and (b) is formulated, following Newns,[10] in terms of the osmotic stress Π, which reduces to zero for fully relaxed polymer. For the assumed case of ideal sorption, we have

$$\mu = \mu^o + RT \ln \tilde{C} + \Pi \bar{V} \tag{4}$$

where $\tilde{C} = C/C_0^\infty$; C_0^∞ is the concentration in the relaxed polymer at equilibrium with $a = 1$; and $\bar{V}$ is the partial molar volume of the sorbed penetrant. Equations 3 and 4 yield

$$\tilde{S} = \frac{\tilde{C}}{a} = \exp\left(-\frac{\Pi \bar{V}}{RT}\right) \tag{5}$$

Note that for the fully relaxed polymer $\tilde{C} = a$ (i.e. $\tilde{S} = 1$).

The viscous deformation of the polymer is governed by a nonlinear form of Newton's law of viscous flow, namely

$$\frac{\partial \epsilon}{\partial t} = k_o \frac{\partial \tilde{C}}{\partial t} = \frac{\Pi}{\eta} = -\frac{RT}{\bar{V}\eta} \ln\left(\frac{\tilde{C}}{a}\right) \tag{6}$$

where[4] ϵ is the deviatory swelling strain, k_o = constant, and the viscosity η is assumed to decrease exponentially with increasing concentration C. Equations 1, 2, and 6 were solved numerically in a consistent manner by an iterative procedure, the rate of convergence of which was not investigated in detail.[4,8]

The JP treatment is not subject to the limitation of assumption a above (thanks to this, a much wider range of non-Fickian kinetic behavior can be satisfactorily interpreted thereby).[5] In particular, it is recognized therein that the unrelaxed glassy polymer *can* (as evidenced by the phenomenon of two-stage sorption)[5,7] accommodate a limited amount of sorbate through fast (practically instantaneous), purely local segmental displacements (in exact analogy with the initial elastic deformation typically observed in viscoelastic mechanical creep behavior).[5] This is done by defining (as illustrated in Figure 1) an "initial" or "instantaneous" sorption isotherm $C^o(a)$ for unrelaxed polymer, in addition to that for fully relaxed polymer considered above, which is here designated by $C^\infty(a)$, the relevant solubility coefficients, for given a, being $S^o = C^o/a$ and $S^\infty = C^\infty/a$. The formulation of the viscous relaxation process is then analogous to that used in Crank's TDD model

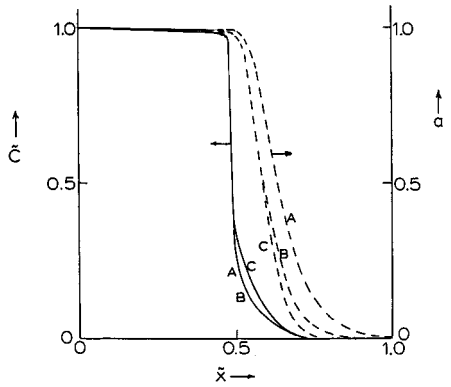

Figure 2. Computed concentration (−) and activity (- - -) penetration profiles for $\tilde{S}^o = S^o/S^\infty = 0.01$ (lines A), 0.1 (B), and 0.2 (C), with $D_F/D_o = 500$, $\tilde{\beta}_o = 10$, and $\beta_F/\beta_o = 10^4$. $\tilde{Q}_t = 0.50_7$ (A), 0.50_1, (B), and 0.50_8 (C).

(but physically it is a closer analogue of the treatment of mechanical viscoelastic deformation than the TDD model),[5] namely

$$\frac{\partial C}{\partial t} = \frac{\partial C^o}{\partial a}\frac{\partial a}{\partial t} + \beta(C^\infty - C) \tag{7}$$

where the relaxation frequency β is taken to be a strongly increasing function of $\tilde{C}$. Equation 7 simply states that incremental penetrant uptake δC (corresponding to the total change in volume swelling strain $\bar{V}\delta C$), over a small time interval δt, can be analyzed into an "elastic" part, which is associated with a corresponding change in activity δa without relaxation, plus a viscous part. The latter corresponds to the amount of penetrant which can be accommodated in the swelling polymer, at constant activity, due to the extra sorptive capacity generated by the relaxation process in time δt.

Equations 1, 2, and 7 can be solved numerically in a straightforward manner.[5] It is worth noting, at this point, that $D_T(C)$ and $\beta(C)$ functions of exponential form were considered in ref 5 as offering the most appropriate compromise between physical reality and mathematical simplicity. Thus, bearing in mind that the concentration dependence of β essentially reflects that of η, there is no significant difference in the formulation of the concentration dependence of the diffusion and viscous relaxation parameters in the TW and JP models. However, because of severe computer power limitations at the time, the actual case II model calculations reported in ref 5 were performed using suitable, computationally less onerous cubic functions for $D_T(C)$ and $\beta(C)$. Although in ref 5 we took care (i) to explain that this course was adopted purely in order to speed up the computation and (ii) to demonstrate the close similarity of the aforementioned cubic functions with the corresponding exponential ones (see Figure 2 therein), a false impression of "empiricism" may have been conveyed to some readers. Accordingly, it is worth stating here that later repetition of typical examples of the computations reported in ref 5 with exponential $D_T(C)$ and $\beta(C)$ functions has invariably led to the expected practically identical results.

Subsequent elimination of assumption a from the TW model by Durning et al. (CD)[11−13] has led to a treatment essentially equivalent to that of JP. The main difference is that the relaxation process is visualized by CD as one

of osmotic stress described by (G_o = instantaneous elastic modulus)

$$\bar{V}\frac{\partial C}{\partial t} = \frac{1}{G_o}\frac{\partial \Pi}{\partial t} + \frac{\Pi}{\eta} = \frac{1}{G_o}\frac{\partial \Pi}{\partial t} + \frac{\beta}{G_o}\Pi \tag{8}$$

instead of the formulation in terms of relaxation of "osmotic strain" adopted by JP in eq 7. Integration of the (assumed linear) elastic term in eq 8 enables us to determine C^o defined above, for a given a, as a function of the corresponding Π, namely[11]

$$\tilde{C}^o = \frac{\Pi}{G_o \bar{V} C_o^\infty} \tag{9}$$

Application of eq 5 then yields the aforementioned "initial" or "instantaneous" sorption isotherm $C^o(a)$, which may be linearized, in a manner consistent with that used for $C^\infty(a)$, by setting $S^o(a) = S^o(a = 1)$ (see Figure 1) to yield

$$\tilde{S}^o = \tilde{C}_o^o = \exp\left(-\frac{G_o \bar{V}^2 C_o^\infty \tilde{C}_o^o}{RT}\right) \tag{10}$$

where $\tilde{C}_o^o = \tilde{C}^o(a = 1)$. Equation 10 illustrates the equivalence of the treatments of JP and of CD.[11] One may either choose a value of G_o and solve eq 10 iteratively for $\tilde{C}_o^o$ or set $\tilde{S}^o$ directly, as was done by JP.

Another similar approach[6] is based on the fact that the compressive DSS imposed by the stiff unpenetrated interior part of the film on the softened swelling outer parts tends to suppress lateral swelling of the latter (i.e., swelling in the plane normal to the penetration axis). This is described by an equation analogous to eq 4 namely[14]

$$\mu = \mu^o + RT \ln \tilde{C} + RTk\sigma \tag{11}$$

where σ is the aforementioned compressive DSS and k is the relevant compliance (note incidentally that the last term in eq 11 is erroneously given in the corresponding equation of ref 14). Equation 11 leads, via eq 3, to the stress dependent solubility coefficient $\tilde{S} = \tilde{C}/a = \exp(-k\sigma)$. Sorption equilibrium (i.e., volume swelling equilibrium) is then attainable via a viscous swelling deformation of the penetrated polymer along $-x$ (the only direction in which the swelling polymer is free to expand), which leads to simultaneous relaxation of σ (ultimately to $\sigma = 0$) and hence to a corresponding increase of $\tilde{S}$, at given a, to $\tilde{S}^\infty = 1$.

All modeling approaches described above (as well as subsequent modeling work of the same nature)[15] typically predict the development of a low-concentration diffuse front (representing diffusion of penetrant in unrelaxed/slowly relaxing polymer) extending ahead of the sharp penetration front referred to above. Theoretical investigation of the shape of the overall case II penetration profile has so far focused largely on the aforesaid diffuse precursor front, assuming a perfectly sharp (steplike) penetration front (cf. Hui et al.[16]).

Experimentally, the presence of such precursor fronts has been demonstrated directly[17−22] or inferred by different methods, such as Rutherford backscattering[17−21] and various optical techniques.[14,22−24] A notable exception is the (otherwise very detailed and informative) investigation by Thomas and Windle[25] of case II diffusion of methyl alcohol (MA) in poly(methyl methacrylate) (PMMA) sheet, by means of microdensitometry, using iodine as colored tracer. In light of strong evidence for precursor fronts provided by Durning et al.[23,24] in a study of case II penetration of MA into very thin supported PMMA films, using a more reliable (even if less direct) interferometric technique, the former authors' failure to detect such fronts is most likely attributable to inability of iodine to penetrate into the low concentration region of the MA penetration profile.

On the other hand, interpretation of the interference pattern obtained by the technique used by Durning et al.[23,24] is model dependent, and these authors have shown that it is not possible to understand important aspects of the observed case II behavior, on the basis of the simple step-cum-exponential precursor front model of Hui et al.[16] (see following paper).

The present and following papers constitute a two-pronged attempt to advance our understanding of the case II diffusion phenomenon, as well as address important specific questions left open by the above experimental work. In part 1, we report significant new theoretical results based on the JP model,[5] concerning both the rate of advance and the overall shape of the case II penetration profile. In particular, a precisely defined relaxation lifetime is evaluated analytically and shown to provide a simple single-parameter link between penetration velocity behavior and relaxation kinetics. In the same vein, a quantitative measure of the steepness of the sharp penetration front, also amenable to analytical evaluation, is proposed and its application illustrated. In part 2, we present the results of an experimental investigation of the case II behavior of the PMMA−MA system, using a different microinterferometric technique, which can yield a reasonably reliable *direct* picture of the penetration profile.

Results of Model Calculations

Model calculations were performed on the basis of eqs 1, 2 and 7, using the approach and computation methods described in detail in ref 5, with only a few minor changes. The notation of ref 5 is also maintained here (note in particular the use of the tilde ~ throughout to denote the dimensionless form of the relevant variables), except for our use of x and β instead of X and β_2 in ref 5.

As in ref 5, we consider symmetric penetration across a film of thickness 2ℓ and confine attention to the half-space $0 \le x \le \ell$. The appropriate boundary condition at $x = \ell$ is then $(\partial a/\partial x)_{x=\ell} = 0$. However, eq 2c may still be satisfied, as nearly as desired, by requiring that $a(x = \ell, t) \to 0$. The other boundary conditions embodied in eqs 2a,b are mere specializations of those of ref 5 (to $a_o = 1$ and $a_1 = 0$, thus making a here equivalent to $\tilde{a}$ in ref 5).

Finally (see Introduction), $D_T(C)$ and $\beta(C)$ are formulated here as exponential functions, namely

$$\tilde{D}_T = \frac{D_T}{D_o} = \exp(k_D C) = \exp(\tilde{k}_D \tilde{C}) \tag{12}$$

$$\tilde{\beta} = \frac{\ell^2 \beta}{D_o} = \tilde{\beta}_o \exp(k_B C) = \tilde{\beta}_o \exp(\tilde{k}_B \tilde{C}) \tag{13}$$

where $D_o \equiv D_T(C = 0)$, $\tilde{\beta}_o \equiv \ell^2\beta(C = 0)/D_o$, k_D = constant, $\tilde{k}_D = k_D C_o^\infty$, k_B = constant, and $\tilde{k}_B = k_B C_o^\infty$.

Calculations were performed, as in ref 5, by application of an explicit finite difference method of solution.

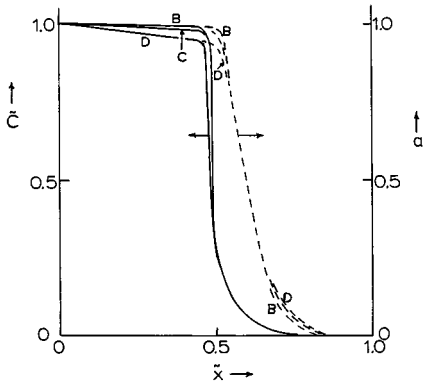

Figure 3. Computed concentration (−) and activity (- - -) penetration profiles for $D(\tilde{C}=1)/D_o = D_F/D_o = 500$ (lines B), 200 (C), and 100 (D), with $\tilde{S}^o = 0.1$, $\tilde{\beta}_o = 10$, and $\beta_F/\beta_o = 10^4$. $\tilde{Q}_t = 0.50_1$ (A), 0.49_4 (B), and 0.51_0 (C).

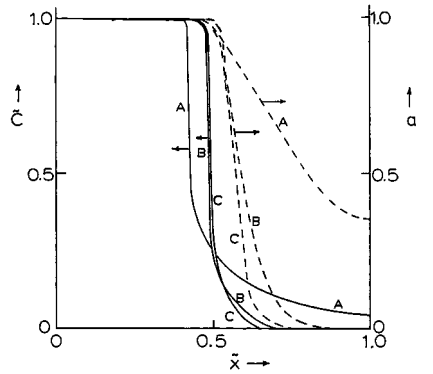

Figure 4. Computed concentration (−) and activity (- - -) penetration profiles for $\tilde{\beta}_o = \ell^2\beta_o/D_o = 1$ (lines A), 10 (B), and 30 (C), with $D_F/D_o = 500$, $\beta_F/\beta_o = 10^4$, and $\tilde{S}^o = 0.1$. $\tilde{Q}_t = 0.49_5$ (A), 0.50_1 (B), and 0.49_7 (C).

An IBM Risc 6000 workstation was used for this purpose. The half space $0 \le \tilde{x} \le 1$ (where $\tilde{x} = x/\ell$) was divided (as in previous analogous work)[4,5] in $N = 20$ intervals ($\Delta\tilde{x} = 1/N = 0.05$), and the time increment $\Delta\tilde{t}$ (where $\tilde{t} = D_o t/\ell^2$) was set, in each case, at a value (in the range 1.5×10^{-8} to 5×10^{-7}) sufficiently low to ensure convergence of the solution.

Values of the remaining salient parameters were chosen[5] in ranges ensuring (within realistic limits of computation accuracy and expense) the establishment of a reasonably extended case II diffusion regime, dictated by the conditions

$$\tilde{\beta}_F \equiv \tilde{\beta}(\tilde{C}=1) \gg \tilde{D}_F \equiv \tilde{D}_T(\tilde{C}=1) \gg \tilde{\beta}_o \gtrsim 1 \quad (14a,b,c)$$

We used $\tilde{D}_F = 100-500$, $\tilde{S}^o = 0.01-0.2$, $\tilde{\beta} = 1-30$, and $\tilde{\beta}_F/\tilde{\beta}_o = 10^3-10^5$.

Penetration Profiles. Examples of the computed penetrant concentration profiles $\tilde{C}(\tilde{x}, \tilde{t} = \text{constant})$ (with $\tilde{t}$ corresponding in each case to a total penetrant uptake, Q_t, equal to ca. half the final equilibrium value, Q_∞, i.e., $\tilde{Q}_t = Q_t/Q_\infty \cong 0.5$) are shown in Figures 2−5 (full lines). The associated activity profiles are also given (broken lines). Bearing in mind that $a = \tilde{C}^\infty$ (see introductory section), the difference $(a - \tilde{C})$ provides a direct measure of how far the system is from complete relaxation at any particular $\tilde{x}$, $\tilde{t}$. The computation becomes increasingly onerous with increasing $\tilde{D}_F$ and/or diminishing $\tilde{S}^o$ (because of the lower Δt values required), while the quality of the data inevitably deteriorates with increasing steepness of the sharp penetration front. A detailed discussion of the latter point is given in ref 5. Figures 2−5 illustrate the effect of each of the aforementioned main parameters ($\tilde{S}^o$, $\tilde{D}_F$, $\tilde{\beta}_o$, or $\tilde{\beta}_F/\tilde{\beta}_o$ respectively), keeping the remaining parameters constant at the values corresponding to the set: $\tilde{S}^o = 0.1$, $\tilde{D}_F = 500$, $\tilde{\beta}_o = 10$, $\tilde{\beta}_F/\tilde{\beta}_o = 10^4$. This "standard set" of parameter values appears in each figure as curve B.

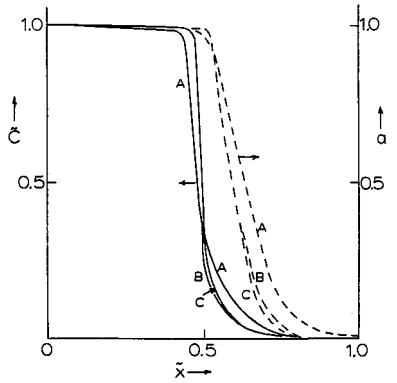

Figure 5. Computed concentration (−) and activity (- - -) penetration profiles for $\beta(C=1)/\beta_o \equiv \beta_F/\beta_o = 10^3$ (lines A), 10^4 (B), and 10^5 (C), with $\tilde{S}^o = 0.1$, $D_F/D_o = 500$, and $\tilde{\beta}_o = 10$. $\tilde{Q}_t = 0.50_5$ (A), 0.50_1 (B), and 0.50_4 (C).

Effect of $\tilde{S}^o = S^o/S^\infty$. Figure 2 shows clearly that rise of $\tilde{S}^o$ from 0.1 (curve B) to 0.2 (curve C) leads to a substantial increase of the height of the precursor front. At the same time, the precursor front becomes steeper and its tail less extended (in line with the somewhat steeper activity profile in case C), so that if the height of the precursor front C is normalized to that of B, the width of the precursor front C would be significantly smaller. As shown more clearly below, this is attributable to a higher effective relaxation frequency, due to the wider concentration range covered by the precursor front C.

It is also noteworthy that (although precursor front height cannot be determined precisely, because of the gradual merging of the precursor, into the sharp, front) the observed height of both precursor fronts B and C, is considerably in excess of the expected value (=0.1 and 0.2 respectively), if the polymer remained unrelaxed in the precursor front region. The role of relaxation in determining precursor front height becomes dominant at values of $\tilde{S}^o$ below 0.1. It is remarkable that not only the height, but the whole precursor front, appears to be little affected by a drop of $\tilde{S}^o$ to a value as low as 0.01, as indicated by the fact that, in Figure 2, precursor front curve A can hardly be distinguished from B. This result (which was confirmed by a study of the intermediate case of $\tilde{S}^o = 0.04$) reflects a compensation effect, in precursor front A, between a lower effective relaxation frequency (due to the more restricted range in concentration) and a correspondingly larger $(a - \tilde{C})$ driving force (clearly apparent in Figure 2), which is consistent with the ubiquitous substantial precursor fronts exhibited by the profiles resulting from the TW model (which corresponds to the case of $\tilde{S}^o \to 0$ here).

Effect of $\tilde{D}_F = D_F/D_o$. In line with relation 14b, the highest value of $\tilde{D}_F$ in the range examined was used for the bulk of our computations. As shown in Figure 3, moderate variation of $\tilde{D}_F$ below this value affects essentially only the high concentration region of the penetration profile. Note in particular that (i) the concentration gradient behind the sharp front (which in this region coincides with the activity gradient)

becomes steeper to compensate for the decrease in $\tilde{D}_F$ and (ii) the steepness of the sharp front tends to decrease to an extent that becomes discernible at $\tilde{D}_F = 100$ (curve D). It is also noteworthy that, for the latter value of $\tilde{D}_F$, a tendency toward negative deviation of the $\tilde{Q}_t$ vs $\tilde{t}$ plot from linearity became increasingly evident, in keeping with the relatively low value of $D_F/\ell^2/\beta_o$.

Effect of $\tilde{\beta}_o = \beta_o/\ell^2/D_o$. Figure 4 shows that $\tilde{\beta}_o$ is the main parameter affecting the width (and secondarily also the height) of the precursor front. In particular, diminution of $\tilde{\beta}_o$ (curves C → B → A) means slower relaxation at low concentrations, on the diffusion time scale, thus allowing more time for the penetrant to diffuse ahead of the sharp front. This is reflected in both concentration and activity profiles. Curve A also shows up a distinct increase of precursor front height. It appears, therefore, that shrinking of the precursor front eventually to the point of undetectability is possible, if $\tilde{\beta}_o$ can be made sufficiently high without infringing conditions.

Effect of β_F/β_o. Figure 5 shows that the effect of β_F/β_o on both concentration and activity profiles is not very significant (cf. curves B, C), as long as the value of this parameter remains sufficiently high to ensure reasonably complete relaxation of the polymer behind the sharp front, as required by condition 14a. Substantially lower values give rise to a more extended precursor front, less steep sharp front and less flat concentration profile behind the sharp front. The fact that the last feature is attributable partly to a less flat activity profile and partly to incomplete relaxation in the region close to the sharp front is well illustrated by curves A.

Case II Penetration Velocities. Dimensionless case II penetration velocities were calculated from the linear part of the computed uptake curves: $\tilde{v}_o = d\tilde{x}_P/d\tilde{t} = d\tilde{Q}_t/d\tilde{t}$ (where $\tilde{x}_P$ denotes the location of the sharp penetration front). As shown in Figure 6, the magnitude of $\tilde{v}_o$ is strongly dependent on $\tilde{\beta}_o$ and is weakly influenced by β_F/β_o. Its sensitivity to $\tilde{S}^o$ is small at low $\tilde{S}^o$ but increases substantially with rising $\tilde{S}^o$.

The slope of the log−log plot of Figure 6a is very close to 0.5, indicating a linear dependence of $\tilde{v}_o$ on $\sqrt{\tilde{\beta}_o}$. This is confirmed by the linear plot of Figure 7. In view of the fact that $\tilde{x} = x/\ell$ and $\tilde{t} = D_o t/\ell^2$, it follows that v_o is linearly related to $\sqrt{\beta_o D_o}$, in line with the analogous results for $\tilde{S}^o \to 0$ derived from the TW model.[4,26,27] The strong correlation of $\tilde{v}_o$ with $\tilde{\beta}_o$, in conjunction with the fact that $\tilde{\beta}_o$ is the principal parameter affecting the precursor profile, provides the physical basis for discussing the behavior of the latter in terms of $\tilde{v}_o$. Thus, curves A → B → C of Figure 4 may be regarded as reflecting the progressive shrinking of precursor front width and height with increasing penetration velocity, in keeping with the behavior predicted by the idealized model of Hui et al.[16] On the other hand, curves A → B → C of Figure 2 are also associated with a significant increase in $\tilde{v}_o$ (see Figure 6b) but the result is rather more complicated, as is discussed in the pertinent text.

Figure 6c points to a linear dependence of log $\tilde{v}_o$ on $\log(\tilde{\beta}_F/\beta_o)$, at constant $\tilde{\beta}_o$, in reasonable agreement with analogous previous results for much lower β_F/β_o values[26] (the relevant slopes are 0.11 and 0.125 respectively).

In an attempt to interpret consistently the behavior of penetration velocity and profile shape revealed by the above results, we proceed to study the kinetic behavior of the relaxation process itself.

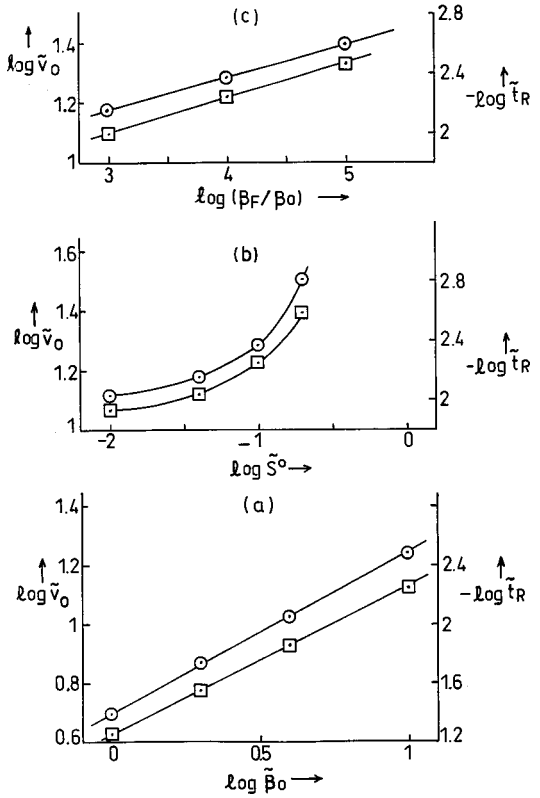

Figure 6. Dependence of computed penetration velocity $\tilde{v}_o$ (circles) and of relaxation lifetime $\tilde{t}_R$ (squares): (a) on $\tilde{\beta}_o$ (with $\tilde{S}^o = 0.1$, $\tilde{D}_F = 200$, $\beta_F/\beta_o = 10^4$); (b) on $\tilde{S}^o$ (with $\tilde{D}_F = 500$, $\tilde{\beta}_o = 10$, and $\beta_F/\beta_o = 10^4$); (c) on β_F/β_o (with $\tilde{S}^o = 0.1$, $\tilde{D}_F = 500$, and $\tilde{\beta}_o = 10$).

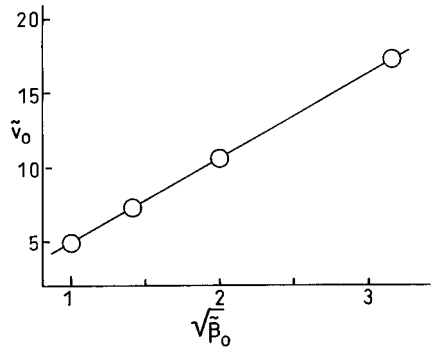

Figure 7. Dependence of computed penetration velocity $\tilde{v}_o$ on $\tilde{\beta}_o = \ell^2\beta_o/D_o$, with $S^o = 0.1$, $D_F/D_o = 200$, and $\beta_F/\beta_o = 10^4$.

Relaxation Kinetics

Here we consider the kinetics of the relaxation process uncomplicated by diffusion, i.e., under conditions of constant activity, such as exist at the exposed surface of the polymer film, where $a = 1$. Thus, we have (cf. eqs 7 and 13)

$$\frac{dC}{dt} = \beta_o \exp(k_B C)(C_o^\infty - C) \qquad (15)$$

where $C(t = 0) = C_o^o$ and $C(t \to \infty) = C_o^\infty$. From eq 15, upon setting $d^2C/dt^2 = 0$, we find that an inflection point (indicating the location of the steepest part of the C vs t curve) exists at

$$C = C_R = C_o^\infty - \frac{1}{k_B} \qquad (16)$$

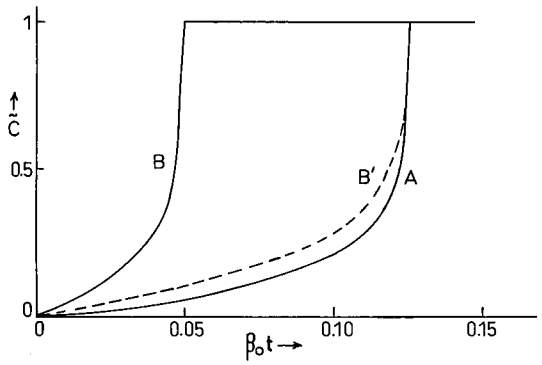

Figure 8. Relaxation kinetics predicted by eq 15 (curve A) and eq l5a (curves B, B′), with $k_H C_o^\infty = k_B C_o^\infty = 9.210$ (corresponding to $\beta_F/\beta_o = \beta'_F/\beta'_o = 10^4$) and $\beta'_o = \beta_o$ (curve B) or $\beta'_o = 2.546\beta_o$ (curve B′) to ensure coincidence of curve A and B at $\tilde{C} = 0.9$.

This point lies in the physically acceptable range of $C_o^o < C_R < C_o^\infty$, if $k_B(C_o^\infty - C_o^o) > 1$, which is equivalent to $\tilde{k}_B(1 - \tilde{S}_o) > 1$. Integration of eq 15 yields

$$t = \frac{1}{\beta_o}\exp(-k_B C_o^\infty) \times \left\{\ln\left(\frac{C_o^\infty - C_o^o}{C_o^\infty - C}\right) + \sum_{n=1}^{\infty}\frac{k_B{}^n[(C_o^\infty - C_o^o)^n - (C_o^\infty - C)^n]}{n!n}\right\} \quad (17)$$

An example of the $C(t)$ curve calculated from eq 17, for a typical value of $\tilde{k}_B = k_B C_o^\infty$ used in the model calculations reported above (and with $C_o^o = 0$), is given by curve A in Figure 8. In view of the very steep approach of C to C_o^∞ and of the closeness of the inflection point to C_o^∞ [eq 16 yields $C_R = 0.89\ C_o^\infty$ for this example and $C_R \rightarrow C_o^\infty$ as $k_B(C_o^\infty - C_o^o) \rightarrow \infty$], a convenient, precisely definable lifetime of the relaxation process is $t_R = t(C = C_R)$. Substitution in eq 17 then yields:

$$t_R = \frac{1}{\beta_I}\exp[-k_B(C_o^\infty - C_o^o)] \times \left\{\ln[k_B(C_o^\infty - C_o^o)] + \sum_{n=1}^{\infty}\frac{k_B{}^n(C_o^\infty - C_o^o)^n - 1}{n!n}\right\}$$

$$\equiv \frac{1}{\beta_I}F[k_B(C_o^\infty - C_o^o)] \equiv \frac{1}{\beta_I}F[\ln(\beta_F/\beta_I)] \quad (18)$$

where (see eq 13)

$$\beta_I = \beta_o \exp(k_B C_o^o) = \beta_o \exp(\tilde{k}_B \tilde{S}^o) \quad (19)$$

An analogous analysis of the relaxation kinetics formulated by TW yields very similar results. In particular, rewriting eq 6 for $a = 1$ in a form closely analogous to eq 15 (and with the assumed[4] concentration dependence of η shown explicitly), we have

$$\frac{1}{C_o^\infty}\frac{dC}{dt} = -\beta'_o \exp(k_H C)\ln\left(\frac{C}{C_o^\infty}\right) \quad (15a)$$

where $\beta'_o = RT/k_o\tilde{V}\eta_o$, $\eta_o/\eta = \exp(k_H C)$, k_H is the material constant corresponding to k_B here, and $\eta_o = \eta(C = 0)$. The resulting inflection point for the concentration range of interest here ($C_o^\infty - C_R \ll C_o^\infty$) is given by

$$\frac{C_R}{C_o^\infty}\ln\left(\frac{C_R}{C_o^\infty}\right) = \frac{1}{k_H} \Rightarrow C_R = C_o^\infty - \frac{1}{k_H}\left(1 + \frac{3}{2k_H C_o^\infty} + ...\right) \quad (16a)$$

It will be noted that, for $k_B = k_H$, eq 16a differs from eq 16 only by the presence of the third and higher terms on the right-hand side, which are small for high values of $\tilde{k}_H = k_H C_o^\infty$.

An illustration of the difference between the relaxation kinetics incorporated in the JP (for $\tilde{S}^o \rightarrow 0$) and TW models is provided by Figure 8; where curves A and B have been calculated, by eq 17 and by numerical integration of eq 15a respectively, with $\beta'_o = \beta_o$ and $\tilde{k}_H = \tilde{k}_B$. These curves exhibit very similar forms and it is only necessary to rescale B (by adjusting β'_o; see curve B′), to achieve satisfactory coincidence of its steep part with that of A and, hence, of the case II behavior predicted by the respective models.

Correlation between Relaxation Kinetics and Case II Diffusion Behavior

Penetration Velocity. Values of the dimensionless form of the relaxation lifetime defined above, $\tilde{t}_R = D_o t_R/\ell^2$, were calculated by means of eqs 18 and 19, as a function of $\tilde{\beta}_o$, $\tilde{S}^o$, and β_F/β_o for the same set of parameter values, as were used for the numerical evaluation of the dimensionless case II penetration velocities $\tilde{v}_o$ shown in Figure 6. The results obtained, also plotted in Figure 6, exhibit trends closely similar to those of $\tilde{v}_o$, suggesting that the behavior of $\tilde{v}_o$ is essentially reducible to that of $\tilde{t}_R$ in all cases. The fact that this is so, to a remarkably high degree of approximation, is demonstrated in Figure 9.

The formulation of eq 18 has been designed to highlight the point that only two parameters are needed to describe the behavior of $\tilde{t}_R$, namely $\tilde{\beta}_I$ and $\tilde{\beta}_F/\tilde{\beta}_I$. Furthermore, the dependence of $\tilde{t}_R$ on β_F/β_I (described by the function F) was found to be much weaker than that on $\tilde{\beta}_I$ (more specifically, over the range of parameter values covered by our computations, $\tilde{\beta}_I$ and β_F/β_I varied by factors of >70 and >60 respectively, resulting in F and $\tilde{t}_R$ varying by factors of <2 and >50, respectively). It follows that, to what still seems a useful degree of approximation (see Figure 10), the behavior of $\tilde{v}_o$ may be described by a single input parameter, namely $\tilde{\beta}_I$. These results constitute a remarkable generalization of that given in Figures 6a and 7.

Concentration Profile. The relaxation kinetics at any location $\tilde{x} > 0$ within the polymer film (subject to the boundary conditions of eq 2) will differ from that described above for $a = 1$, primarily because the activity a at $\tilde{x}$ is initially zero and can only rise at a finite rate dictated by the rate at which the diffusing penetrant arrives at that location. As illustrated in Figure 11, however, $a(\tilde{x}, \tilde{t})$ tends to attain the final value a_B before the final sharp rise of $\tilde{C}$ to $\tilde{C}_B^\infty = a_B$; where $a_B \cong 1$, provided that the penetration rate is not subject to significant diffusion limitation effects (as required by condition 14b). One should also note that, under conditions of case II kinetics, $\tilde{C}(\tilde{x} = \text{const}, \tilde{t})$ curves of the type shown in Figure 11 can be simply transformed to the corresponding concentration profile $\tilde{C}(\tilde{x} = \text{constant}, \tilde{t})$ via the relation

$$\left(\frac{\partial\tilde{C}}{\partial\tilde{x}}\right)_{\tilde{t}} = -\frac{1}{\tilde{v}_o}\left(\frac{\partial\tilde{C}}{\partial\tilde{t}}\right)_{\tilde{x}} \quad (20)$$

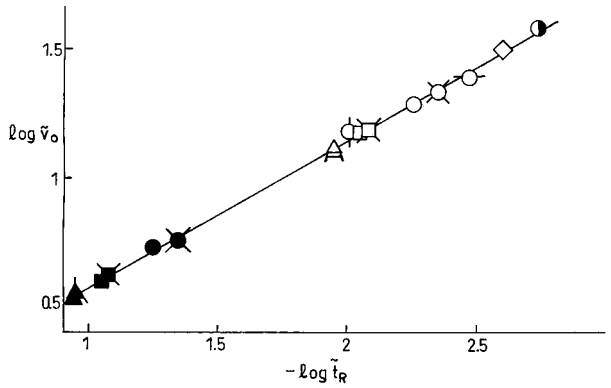

Figure 9. Correlation between computed penetration velocity $\tilde{v}_o$ and relaxation lifetime $\tilde{t}_R$ for $\tilde{D}_F = 500$: $\tilde{S}^o = 0.01$ (triangles), 0.04 (squares), 0.1 (circles), 0.2 (diamond); $\tilde{\beta}_o = 1$ (fully shaded), 10 (unshaded), 30 (half shaded); $\beta_F/\beta_o = 10^4$, except for $\beta_F/\beta_o = 10^3$ (○ with two vertical bars), 10^5 (○ with two horizontal bars); $\beta_F/\beta_I = 10^4$ (open or solid characters with three or more bars).

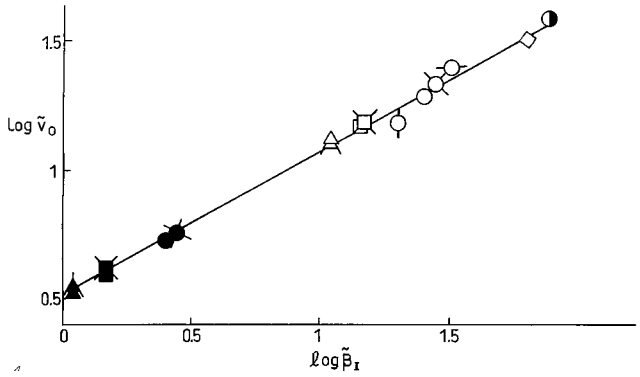

Figure 10. Correlation between computed penetration velocity $\tilde{v}_o$ and $\tilde{\beta}_I$. Significance of points as in Figure 9.

Accordingly, for a flat high concentration profile and a not too prominent precursor front, the shape of the sharp front is determined by the relaxation kinetics for $a \cong 1$ considered in the preceding section. In particular, the steepness of the said sharp front may be usefully characterized by the magnitude of its slope at the inflection point. Thus, on the basis of eqs 15, 16, and 20, we have

$$\left(\frac{\partial \tilde{C}}{\partial \tilde{x}}\right)_{\tilde{C}=\tilde{C}_R} \cong -\frac{\tilde{\beta}_o}{\tilde{v}_o \tilde{k}_B}\exp(\tilde{k}_B - 1) = -\frac{\tilde{\beta}_F \exp(-1)}{\tilde{v}_o \ln(\beta_F/\beta_o)} \quad (21)$$

$$\left(\frac{\partial C}{\partial x}\right)_{C=C_R} \cong -\frac{\beta_o}{v_o k_B}\exp(k_B C_o^\infty - 1) = -\frac{\beta_F}{v_o k_B \exp(1)} \quad (21a)$$

in terms of dimensionless and experimental variables, respectively.

Referring back to the discussion of the model calculation results, note that the change in sharp front steepness predicted by eq 21, when $\tilde{\beta}_F$ is varied (at constant $\tilde{\beta}_o$), becomes clearly visible in Figure 5 at lower $\tilde{\beta}_F$ values (cf. curves A and B representing $\tilde{\beta}_F = 10^4$ and $\tilde{\beta}_F = 10^5$ respectively). Note also, for completeness, that in the aforementioned example there are small opposing effects, due to concurrent changes in $\tilde{k}_B$ and $\tilde{v}_o$, which are easily overridden by that of $\tilde{\beta}_F$ The situation is somewhat different when $\tilde{\beta}_o$ is varied (at constant β_F/β_o). Thus, a 10-fold change of $\tilde{\beta}_o$ (cf. curves A and B of Figure 4 representing $\tilde{\beta}_o = 1$ and $\tilde{\beta}_o = 10$, respectively) is

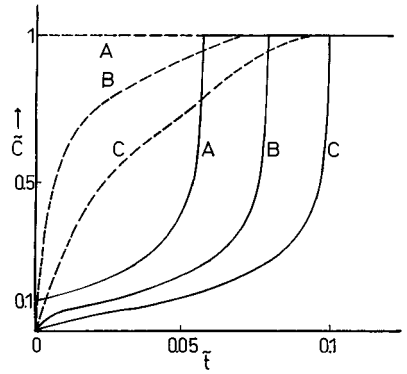

Figure 11. Examples of the evolution of concentration (full lines) and activity (broken lines) at various locations in the polymer film: $\tilde{x} = 0$ (curves A), 0.1 (B), and 0.2 (C); $\tilde{D}_F = 500$, $\tilde{S}^o = 0.1$, $\tilde{\beta}_o = 10$, and $\beta_F/\beta_o = 10^4$.

accompanied by an opposing relatively large (nearly 4-fold, see Figure 6a) change in $\tilde{v}_o$. It is not surprising, therefore, that the resulting effect on sharp front steepness is not so easily discernible. One may further note that the tendency of the sharp front to become less steep with decreasing $\tilde{D}_F$ (illustrated by curves B → D in Figure 3) is in line with the accompanying increase of the concentration gradient in the relaxed polymer region. The maximum attainable concentration ($\tilde{C}_B^\infty = a_B$) in the sharp front region is thus lowered as $\tilde{D}_F$ is reduced; hence, $\tilde{\beta}_F$ in eq 21 should be replaced by $\tilde{\beta}_B = \tilde{\beta}(\tilde{C}_B^\infty) < \tilde{\beta}_F$.

Summary and Conclusions

The JP relaxation-dependent solubility model[5] has been used here as a basis for a more detailed systematic exploration of the predicted dependence of penetration velocity and of salient features of the concentration profile, on the principal parameters governing case II behavior. In particular, the variation of $\tilde{v}_o$ and of the sharp and diffuse parts of the concentration profile, as a function of each of the said parameters, namely $\tilde{D}_F$, $\tilde{S}^o$, $\tilde{\beta}_o$, and $\tilde{\beta}_F/\tilde{\beta}_o$ has been studied by means of appropriate model calculations, after restoring the (physically more appropriate) exponential form to the concentration dependence of D_T and β (since computer limitations, which imposed the use of simpler functions for this purpose in ref 5, no longer exist). The results obtained fully confirm and substantially extend previous results obtained from simpler models.[4,16,26]

A comparative discussion of the models of the TW and JP models[4,5] has been given to elucidate their similarities and differences and to justify our choice of the latter for the present work. Thus, it has been shown that the general physical basis and the salient features of relaxation kinetics are very similar. However, the presence of the parameter $\tilde{S}^o$ in the JP model confers on it substantial advantages, notably (i) a closer approach to physical reality leading to much wider applicability, (ii) greater computational rigor and simplicity, and (iii) analytical tractability of the all-important relaxation lifetime parameter.

Relaxation kinetics was studied separately. It was shown that a remarkably close and simple single-parameter link between the aforementioned behavior of penetration velocity and relaxation kinetics, is provided by a precisely definable characteristic relaxation lifetime t_R. The latter parameter is closely analogous to the yield delay time in mechanical creep experi-

ments.[28] Use of this concept has previously been made in our semiquantitative interpretation of the wide variety of kinetics (ranging from case I to case II), which characterize penetration of strong swelling agents in various directions along uniaxially oriented cellulose acetate films;[29,30] however, the present results confer quantitative substance to the said concept. To a lower, but still very useful, degree of approximation, the behavior of $\tilde{v}_o$ may be interpreted in terms of a single *input* parameter, namely $\tilde{\beta}_I$. It is noteworthy that the slope of the log−log correlations shown in Figures 9 and 10 is the same as that of Figure 6a. This means that the functional form of the dependence of $\tilde{v}_o$ on $\tilde{t}_R$ or β_I is the same as that of the previously established[4,16,26] dependence of $\tilde{v}_o$ on $\tilde{\beta}_o$. Thus, the former two results represent true generalizations of the latter one. On this basis, it appears that the conditions of case II kinetics embodied in relation 14 should properly be written in terms of $\tilde{t}_R$ rather than of $\tilde{\beta}_o$.

A quantitative measure of the steepness of the sharp part of the concentration profile has also been devised and expressed analytically in terms of relaxation kinetic parameters. The resulting expression has been used to interpret certain visible changes in our computed sharp profiles; but its real utility stems from the fact that simple numerical computation constitutes a very inefficient way of obtaining information of this kind. The difficulty posed by the inevitable coarseness of the subdivision of x may be circumvented by reverting to $C(\tilde{x} = \text{constant}, \tilde{t})$ curves of the type illustrated in Figure 11 (which are computed over very small time intervals), but the problem of the inaccuracy of the numerical approximations in the region of the sharp front (at any *practical* $\Delta\tilde{x}$ value) remains. The aforementioned expression also has considerable practical utility, especially with regard to the evaluation of the results of experimental techniques,[23,24] which are sensitive to (and are potentially capable of providing information on) even subtle changes of sharp profile steepness. This matter is taken up in part 2.

Notation

a: activity of penetrant defined by eq 3
C: concentration of penetrant in mol per unit volume of pure polymer
$C^o(a)$: sorption isotherm for unrelaxed polymer
$C^\infty(a)$: sorption isotherm for fully relaxed polymer
C_o^o: concentration in the unrelaxed polymer at $a = 1$
C_o^∞: concentration in the fully relaxed polymer at $a = 1$
C_R: concentration at the inflection point of the relaxation kinetic C vs t curve
$\tilde{C}[=C/C_o^\infty]$: normalized concentration
D_T: thermodynamic diffusion coefficient defined here on a polymer-fixed frame of reference
$D_o[=D_T(C = 0)]$: thermodynamic diffusion coefficient at the limit of zero concentration
D_F: thermodynamic diffusion coefficient at $C = C_o^\infty$
$\tilde{D}_F[=D_F/D_o]$: normalized thermodynamic diffusion coefficient at $C = C_o^\infty$
G_o: instantaneous elastic modulus.
k: compressive compliance
k: constant in eq 13
k_D: constant in eq 12
k_H: material constant in eq 15a
k_o: constant in eq 6
$\tilde{k}_B[=k_BC_o^\infty]$: constant in eq 13
$\tilde{k}_D[=k_DC_o^\infty]$: constant in eq 12
ℓ: half thickness of film
Q_t, Q_∞: penetrant uptake at t and $t \rightarrow \infty$ respectively
$\tilde{Q}_t[=Q_t/Q_\infty]$: normalized penetrant uptake
$S[=C/a]$: solubility coefficient
$S^o[=C^o/a]$: solubility coefficient corresponding to unrelaxed sorption isotherm
$S^\infty[=C^\infty/a]$: solubility coefficient corresponding to fully relaxed sorption isotherm
$\tilde{S}[=\tilde{C}/a]$: normalized solubility coefficient
$\tilde{S}^o[=S^o/S^\infty]$: ratio of linearized unrelaxed and fully relaxed sorption isotherms
t: time
$t_R[=t(C = C_R)]$: lifetime of the relaxation process
$\tilde{t}[=D_ot/\ell^2]$: dimensionless time
$\tilde{t}_R=[D_ot_R/\ell^2]$: dimensionless lifetime of the relaxation process
$\Delta\tilde{t}$: dimensionless time increment used in computations
$\bar{V}$: partial molar volume of the sorbed penetrant
$\tilde{v}_o[=d\tilde{x}_P/d\tilde{t} = d\tilde{Q}_t/d\tilde{t}]$: dimensionless case II penetration velocity
x: position along the axis of penetration
$\tilde{x}[=x/\ell]$: dimensionless position coordinate
$\tilde{x}_P$: dimensionless location of the sharp penetration front
$\Delta\tilde{x}$: dimensionless space increment used in computations

Greek Symbols

β: relaxation frequency defined in eq 7
β_o: $\beta(C = 0)$
β_I: $\beta(C = C_o^o)$
β_F: $\beta(C = C_o^\infty)$
β'_o: relaxation frequency defined in eq 15a
$\tilde{\beta}[\beta\ell^2/D_o]$: dimensionless relaxation frequency
ϵ: deviatory swelling strain defined in eq 6
η: viscosity
μ, μ^o: chemical potential of penetrant in the polymer and in the pure bulk liquid respectively
Π: osmotic stress
σ: compressive differential swelling stress

References and Notes

(1) Alfrey, T.; Gurnee, E. F.; Lloyd, W. G. *J. Polym. Sci., Part C* **1966**, *12*, 249.
(2) Crank, J. *J. Polym. Sci.* **1953**, *11*, 151.
(3) Hopfenberg, H. B.; Stannett, V. In *The Physics of Glassy Polymers*; Haward, R. N., Ed.; Applied Science Publ.: London, 1973; Chapter 9.
(4) Thomas, N. L.; Windle, A. H. *Polymer* **1982**, *23*, 529.
(5) Petropoulos, J. H. *J. Polym. Sci., Part B: Polym. Phys. Ed.* **1984**, *22*, 1885.
(6) Petropoulos, J. H. *J. Polym. Sci., Part B: Polym. Phys. Ed.* **1984**, *22*, 183.
(7) Petropoulos, J. H.; Roussis, P. P. In *Permeability of Plastic Films and Coatings to Gases, Vapors and Liquids;* Hopfenberg, H. B., Ed.; Plenum: New York, 1974; p 219.
(8) Windle A. H. In *Polymer Permeability;* Comyn, J., Ed.; Elsevier Applied Science Publishers: London, 1985; p 75.
(9) Petropoulos, J. H.; Roussis, P. P. *J. Chem. Phys.* **1967**, *47*, 1491.
(10) Newns, A. C. *Trans. Faraday Soc.* **1956**, *52*, 1533.
(11) Durning, C. J. *J. Polym. Sci., Part B: Polym. Phys. Ed.* **1985**, *23*, 1831.
(12) Durning, C. J.; Tabor, M. *Macromolecules* **1986**, *19*, 2220.
(13) Huang S. J.; Durning C. J. *J. Polym. Sci., Part B: Polym. Phys. Ed.* **1997**, *35*, 2103.
(14) Sanopoulou M.; Petropoulos, J. H. *J. Polym. Sci: Part B: Polym. Phys. Ed.* **1988**, *26*, 1087.
(15) Wu, J. C.; Peppas, N. A. *J. Polym. Sci: Part B: Polym. Phys. Ed* **1993**, *31*, 1503; *J. Appl. Polym. Sci.* **1993**, *49*, 1845.

(16) Hui, C. Y.; Wu, K. C.; Lasky, R. C.; Kramer, E. J. *J. Appl. Phys.* **1987**, *61*, 5137.
(17) Mills, P. J.; Palmstrom, C. J.; Kramer, E. J. *J. Mater. Sci.* **1986**, *21*, 1479.
(18) Mills, P. J.; Kramer, E. J. *J. Mater. Sci.* **1986**, *21*, 4151.
(19) Hui, C. Y.; Wu, K. C.; Lasky, R. C.; Kramer, E. J. *J. Appl. Phys.* **1987,** *61*, 5129.
(20) Lasky, R. C.; Kramer, E. J.; Hui, C. Y. *Polymer* **1988**, *29*, 637.
(21) Lasky, R. C.; Kramer, E. J.; Hui, C. Y. *Polymer* **1988**, *29*, 1131.
(22) Sanopoulou M.; Petropoulos, J. H. *J Polym. Sci: Part B: Polym. Phys. Ed* **1992**, *30*, 983.
(23) Durning, C. J.; Hassan, M. M.; Tong, H. M.; Lee, K. W. *Macromolecules* **1995**, *28*, 4234.
(24) Hassan, M. M.; Durning, C. J. *J Polym. Sci: Part B: Polym. Phys. Ed.* **1999**, *37*, 3159.
(25) Thomas, N.; Windle, A. H. *Polymer* **1978**, *19*, *255.*
(26) Fu, T. Z.; Durning, C. J. *AIChE J.* **1993**, *39*, 1030.
(27) Durning, C. J.; Edwards, D. A.; Cohen, D. S. *AIChE J* **1996**, *42*, 2025.
(28) E.g.: Matz, D. J.; Guldemond, W. G.; Cooper, S. L. *J. Polym. Sci.* **1972**, *10*, 1917.
(29) Sanopoulou, M.; Petropoulos, J. H. J *Polym. Sci., Part B, Polym. Phys.* **1992**, *30*, 983.
(30) Sanopoulou, M.; Petropoulos, J. H. *J. NonCryst. Solids* **1991**, *131*−*3*, 827.

MA001408J